Journal of Power Sources 244 (2013) 294–299

Contents lists available at SciVerse ScienceDirect

Journal of Power Sources

journal homepage: www.elsevier.com/locate/jpowsour

Heat generation behavior during charging and discharging of lithium-ion batteries after long-time storage

Yoshiyasu Saito [a,*], Masahiro Shikano [a,b], Hironori Kobayashi [a,b]

[a] Energy Technology Research Institute, National Institute of Advanced Industrial Science and Technology (AIST), AIST Tsukuba Central 2, 1-1-1 Umezono, Tsukuba, Ibaraki 305-8568, Japan
[b] Research Institute for Ubiquitous Energy Devices, National Institute of Advanced Industrial Science and Technology (AIST), 1-8-31 Midorigaoka, Ikeda, Osaka 563-8577, Japan

HIGHLIGHTS

- We characterize the heat generation behavior of degraded lithium-ion batteries.
- The more degraded batteries shows larger heat generation at higher rates charging and discharging.
- The main reason for increase in the heat generation is increase in the inner resistance.
- The characteristics for the post-degradation state should be considered in the thermal design.

ARTICLE INFO

Article history:
Received 29 October 2012
Received in revised form
21 December 2012
Accepted 24 December 2012
Available online 12 January 2013

Keywords:
Lithium-ion battery
Heat generation
Calorimetry
Degradation
Storage test

ABSTRACT

Thermal design and management are important for lithium-ion batteries (LIBs) to prevent thermal runaway under normal and abnormal conditions such as overcharge and short circuit. A sound understanding of the heat generation behaviors of LIBs is needed for their thermal design and management. Since battery characteristics such as capacity and power capability degrade with time and the number of cycles, one can infer that the amount of heat generated by LIBs may also be changed by this degradation. Calorimetry is an effective method of studying the heat generation mechanisms of LIBs. In this study, we apply calorimetry to characterize the heat generation behavior of LIBs during charging and discharging after degradation due to long-time storage. At low rates of charging and discharging, such as 0.1*C*, significant differences dependent on the degree of degradation are not observed. On the contrary, more degraded batteries exhibit greater heat generation related to overvoltage increase at high rates of charging and discharging, such as 1 *C*. The solution resistance increase is particularly striking in an LIB stored at 50 °C. The chief cause of this increase may be leakage of electrolyte solution, resulting in greater heat generation at high rates of charging and discharging.

1. Introduction

The thermal design and thermal management of lithium-ion batteries (LIBs) are important for ensuring their safety and the reliability. Some safety tests such as nail penetration and overcharge are generally conducted on fresh batteries before their commercialization [1,2]. Of course, safety has to be ensured for batteries over their entire lifetime. The thermal behavior of both fresh and degraded batteries should be factored into the thermal design of batteries. However, there are a few reports on safety tests for LIBs degraded after long-time use.

Abnormal states such as short circuit and overcharge are critical for battery safety. However, we should also monitor the heat generation behavior of LIBs under normal conditions to see if it changes gradually owing to degradation. In our previous studies on LIB degradation, we found some variations at the electrode surface, particularly the positive side [3–9]. Building up of surface materials formed by electrolyte decomposition and a structural change of the active material from a hexagonal layered oxide to a Li-deficient cubic phase were typical variations characteristic of the degraded states. These phenomena might also affect the thermal behavior of the battery through resistance increase and capacity fading. In this study, we investigate the heat generation behavior of LIBs during charging and discharging after degradation by long-time storage and consider the impact on battery performance.

2. Experimental

Cylindrical LIBs (18650-type) were prepared as test sample cells whose main constituent materials were the same as in past studies

* Corresponding author.
E-mail address: y-saito@aist.go.jp (Y. Saito).

0378-7753/$ – see front matter © 2013 Elsevier B.V. All rights reserved.
http://dx.doi.org/10.1016/j.jpowsour.2012.12.124

[10]. $LiNi_{0.8}Co_{0.15}Al_{0.05}O_2$ (NAT) from Toda Kogyo was selected as the active material of the positive electrode. The electrode also contained 7 wt% of polyvinylidene fluoride (PVDF) binder (KF1300, Kureha) and 7 wt% of acetylene black (HS-100, Denki Kagaku Kogyo) as a conductive agent. Hard carbon (Carbotron® PS(F)) from Kureha was used in the negative electrode as the active material with the other PVDF binder (KF1100, Kureha). The weight ratio of hard carbon to binder was 10.5:9.5 in the negative electrode. The electrolyte (LIPASTE-E2DMC/PF1, Tomiyama Pure Chemical) was a mixed solvent of ethylene carbonate (EC) and dimethyl carbonate (DMC) containing 1 mol dm^{-3} of $LiPF_6$, where the volume ratio of EC to DMC was 1:2.

Three types of characteristics, namely, discharging capacity, DC resistance, and AC impedance, were selected as indices of battery performance. The standard condition of discharge was a constant current of 450 mA (1*C* rate), and the cutoff voltage was 2.5 V. In addition, the charging condition consisted of two phases in which constant current charging of 450 mA was followed by constant voltage charging at 4.1 V after the cell voltage was increased to 4.1 V, and the total charging time was 3 h. The DC resistance of the cell was evaluated from the relation between the current and the voltage. In this evaluation, four kinds of currents (0.45, 1.35, 2.25, and 4.5 A) were applied to the LIBs, and the voltages 10 s after the application of the currents were analyzed. For the AC impedance measurement, the applied voltage was 5 mVp-p, and the frequency range was between 100 kHz and 10 mHz. The DC resistance and AC impedance were measured only at an SOC of 30%. The standard temperature of these measurements was 25 °C. A battery testing system (TOSCAT-3200, Toyo system) was used for the measurements of discharging capacity and DC resistance, and the AC impedance was measured using a multichannel potentiostat (CellTest 1470E, Solartron) combined with a frequency response analyzer (CellTest 1400A, Solartron).

In the storage test, one cell was stored at 50 °C and the other cell at 25 °C. The SOC of both cells was set to 90% before the storage test, which was controlled by constant current charging of 450 mA followed by charging with a constant voltage of 3.971 V. Thermostat chambers (SU220, Espec) were used to control the temperature. After 436 days of storage, the test was terminated owing to the unexpected occurrence of the Great East Japan Earthquake, and the cells were kept at room temperature for approximately 300 days, after which they were submitted for calorimetric measurement. Another cell that had been stored at an SOC of 50% for 652 days at 20 °C was also submitted for calorimetry. Table 1 summarizes the conditions of the storage test of the sample cells.

Heat generation during the charging and discharging of the degraded cells after the storage test was measured by using a twin-type heat conduction calorimeter (C80-22, Setaram). The sample cell fitted in the sample holder at the sample side of the calorimeter was connected to the external battery testing system (TOSCAT-3200) through lead wires for charging and discharging. A brass dummy cell whose heat capacity was comparable to that of the sample cell was used as the reference and was fitted in another sample holder at the reference side of the calorimeter. Heat loss through the wires was 1% or less in this system. The time constant of the thermal response delay τ was approximately 515 s, and the influence of the delay was corrected in the analysis. The temperature of the calorimeter was maintained constant at 25 °C.

Table 1
Conditions of the storage test.

Sample cells	(A)	(B)	(C)
Temperature (°C)	50	25	20
SOC (%)	90	90	50
Time (days)	436	436	652
Storage time at RT after the, test (days)	286	312	0

Table 2
Initial characteristics of the sample cells.

Sample cells	(A)	(B)	(C)
Weight (g)	35.331	35.317	–
Discharging capacity (mAh)	472.7	481.8	476.9
DC resistance of discharge (SOC = 30%) (mΩ)	80.8	79.7	–
DC resistance of discharge (SOC = 50%) (mΩ)	68.3	66.0	72.3
Power capability (SOC = 30%) (W)	27.3	27.7	–
Power capability (SOC = 50%)(W)	43.2	45.1	41.2

3. Results and discussion

The cell characteristics before and after the storage test are listed in Tables 2 and 3, respectively. In the initial state, the three sample cells show similar characteristics. After the storage test, striking degradation is observed in all the samples. Higher temperature causes greater degradation of the capacity during storage. The results of the test samples show that degradation of power capability is more critical than capacity fading, particularly at higher temperatures. Fig. 1 shows the complex plane plots of the AC impedance of the cells after the storage test. All plots crossed the horizontal axis at approximately 1 kHz in the applied frequency. A semicircle is remarkably seen in the frequency range between 1 and 50 Hz, and at least one smaller semicircle is observed in the higher-frequency region. The impedance in the lower-frequency region less than 0.1 Hz is rising to the right and might be controlled by diffusion of lithium ions. The equivalent circuit model shown in Fig. 2 was used to fit the obtained impedance spectra for the limited frequency range between 0.1 Hz and 2 kHz, following the work of Seki and co-workers [11,12]. In this model, L is the inductance caused by the shape of the electrodes, which are spirally wounded in the cylindrical cell case. The resistance element R_s is the solution resistance, and R_{ct1} and R_{ct2} are the charge transfer resistances at the interfaces of the electrodes and the electrolyte. However, R_s includes the electronic resistance of the conductive components in the batteries, such as the current collectors and the contact resistances between those components, as well as the ionic resistance of the electrolyte. The constant phase element, CPE_{dl}, was used in this model instead of the double-layer capacitor at the electrode interface, taking into account the roughness of the electrode surface. We also used another constant phase element, CPE_{dif}, for the diffusion resistance, but not for the Warburg impedance. Two *RC* parallel circuits, R_{ct1}—CPE_{dl1} and R_{ct2} CPE_{dif}—CPE_{dl2}, correspond to the interface reactions of the negative and the positive electrodes, and the semicircles in Fig. 1 are drawn by these elements. The values of the resistor elements of the equivalent circuit estimated from the fitting were summarized in Table 4. The result suggests that the greater increase in the DC resistance after 50 °C storage is mainly caused by an increase in the solution resistance, R_s, and therefore degradation of the electrolyte. On the contrary, R_s slightly

Table 3
Degraded characteristics of the sample cells after the storage test.

Sample cells	(A)	(B)	(C)
Weight (g)	35.083	35.255	–
Weight retention	0.993	0.998	–
Discharging capacity (mAh)	407.4	448.7	467.8
Capacity retention	0.862	0.931	0.981
DC resistance of discharge (SOC = 30%) (mΩ)	171.8	90.2	96.0
Power capability (SOC = 30%) (W)	12.9	24.5	22.9
Power retention	0.473	0.884	–

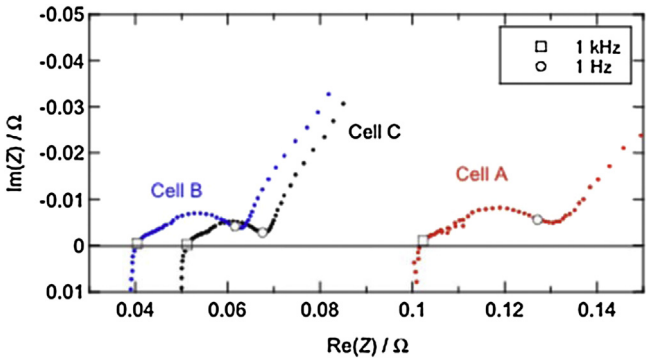

Fig. 1. Complex plane plot of AC impedance of the sample cells at 25 °C; SOC = 30%.

decreased in storage at 25 °C. This may be due to the difference in the contact resistance between the sense terminals and the battery package (the positive and the negative terminals). Both charge transfer resistances, R_{ct1} and R_{ct2}, showed a rising trend for the storage, and this result suggests that both interface structures at the positive and the negative electrodes gradually changed during storage. An especially large variation was shown in R_{ct2} after the storage at 50 °C. Higher temperatures such as 50 °C appear to accelerate the increase in R_{ct2} and the consequent power fading. In past studies, it was found that, remarkably enough, the increase in charge transfer resistance occurred at the positive side in degraded cells, which was attributed to a variation in the surface structure of the positive electrode material [3–8]. A lithium-deficient cubic phase was formed on the surface of the active material [4,8], and materials containing carbonyl formed by electrolytic decomposition, such as lithium alkyl carbonate, are deposited on the electrode surface [5,6]. In the present cells, the same reactions should occur at the interface of the positive electrode, resulting in an increase in R_{ct2}.

The DC resistance of cell C is greater than that of cell B after the storage test. However, R_{ct1} and R_{ct2} exhibit an inverse relationship. Apparently, the difference in the solution resistance has a greater impact than the charge transfer resistances in the sample cells. As is clear from a comparison of Tables 2 and 3, a slight weight loss in the cells is observed after storage, and this suggests that a small amount of the electrolyte solvent might have vaporized and leaked out of the cell during storage, particularly at the elevated temperature. A gray deposit that appears on the cap of cell A after the storage at 50 °C might be mixtures of lithium compounds of LiF, LiOH, Li_2CO_3, and so on, formed by a reaction between exuded $LiPF_6$ and water vapor in the atmosphere. The elevated temperature may weaken the sealing of the cell, resulting in leakage of the electrolyte and weight loss of the cell.

Fig. 3 shows the voltage and heat generation profiles of the sample cells during constant current charging and discharging of 45 mA. In the voltage profiles, the difference between charging and discharging voltages is large in the low-SOC region, which is

Table 4
Impedance parameters of the cells before and after the storage test.

Sample cells	R_s (mΩ)			R_{ct1} (mΩ)			R_{ct2} (mΩ)		
	$R_{s,bef}$	$R_{s,aft}$	ΔR_s	$R_{ct1,bef}$	$R_{ct1,aft}$	ΔR_{ct1}	$R_{ct2,bef}$	$R_{ct2,aft}$	ΔR_{ct1}
(A)	38.4	109.4	71.0	5.0	8.9	3.9	11.2	23.0	11.8
(B)	40.6	37.9	−2.7	2.9	7.3	4.4	12.6	17.4	4.8
(C)	ND	49.4	ND	ND	5.4	ND	ND	13.2	ND

Note: The subscripts "bef" and "aft" mean "before" and "after" storage tests, respectively; ND: No data.

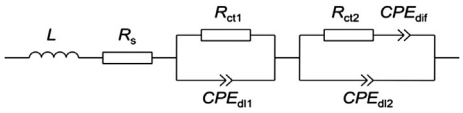

Fig. 2. The equivalent circuit of the sample cells.

a typical characteristic of cells using a hard carbon negative electrode [13]. It appears that the cell stored at 50 °C shows slightly greater heat generation than the other cells, particularly in the high-SOC region, during charging. However, the difference is not very large, and it is difficult to diagnose the degradation of the cell from the calorimetric results at such a low rate of cycling.

If side reactions are negligible, the heat generation from an electrochemical cell, P, during constant current charge and discharge is described as

$$P = \mathrm{IT}\left(\frac{\partial V_{\mathrm{OCV}}(\mathrm{SOC})}{\partial T}\right)_p + I(V(\mathrm{SOC}, I) - V_{\mathrm{OCV}}(\mathrm{SOC})) \quad (1)$$

where current I is positive in the charging direction [14–17]. Parameters V, V_{ocv}, and T are the working voltage, open circuit voltage

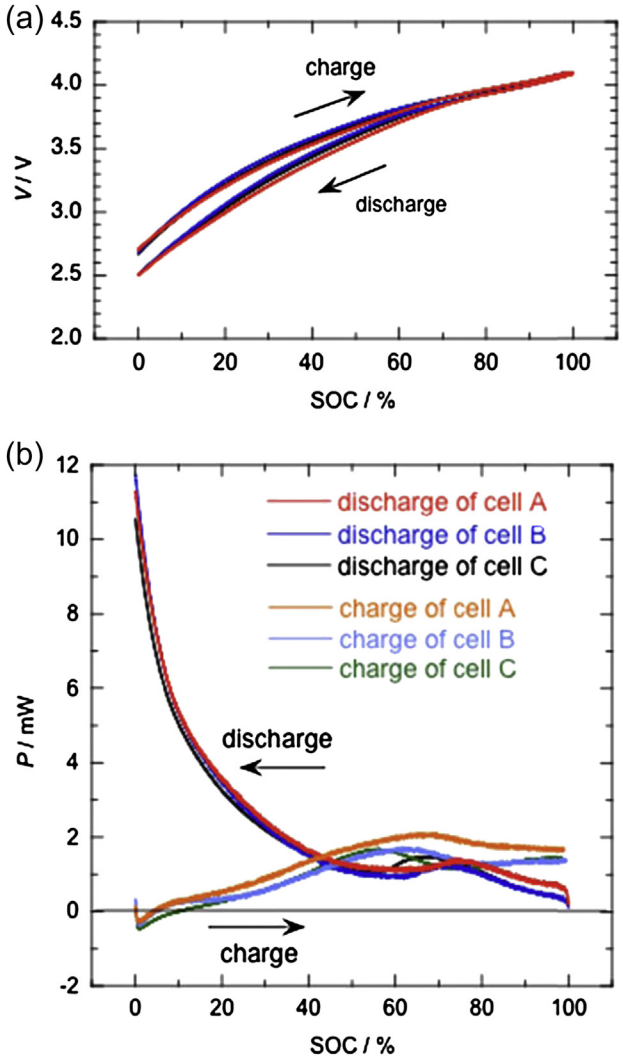

Fig. 3. (a) Voltage V (V) and (b) heat flow P (mW) profiles of the sample cells during charging and discharging of the constant current at 45 mA. The temperature is 25 °C.

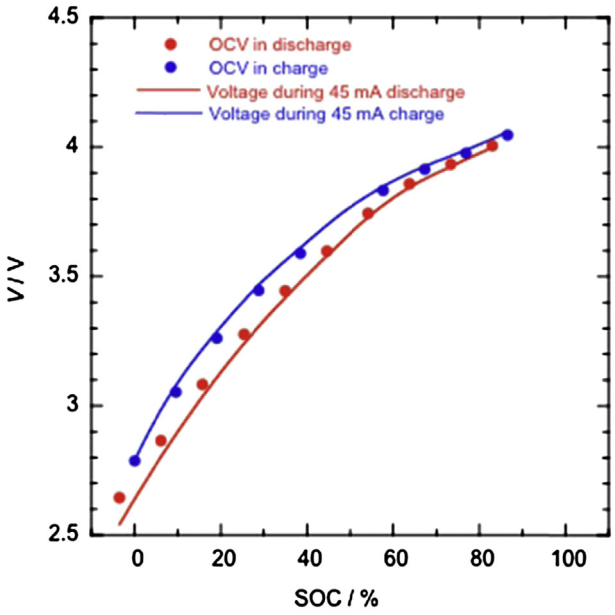

Fig. 4. The open circuit voltage, OCV (V), of cell C measured by intermittent charging and discharging, and the voltage V (V) during constant current charging and discharging at 45 mA.

(OCV), and temperature, respectively. Another form of the equation is as follows:

$$P = \frac{\mathrm{IT}\Delta(\mathrm{SOC})}{nF} + I\eta(I) = P_\mathrm{s} + P_\mathrm{r} \quad (2)$$

The first term, P_s, is the heat from the cell reaction itself at a given time, which is related to the partial entropy change of the cell reaction, $\Delta s(\mathrm{SOC})$. Parameter n is the number of electrons for the cell reaction, which is unity for the sample cells, and F is Faraday's constant. The second term, P_r, is the heat from the energy loss due to overvoltage at a given time, which originates in the

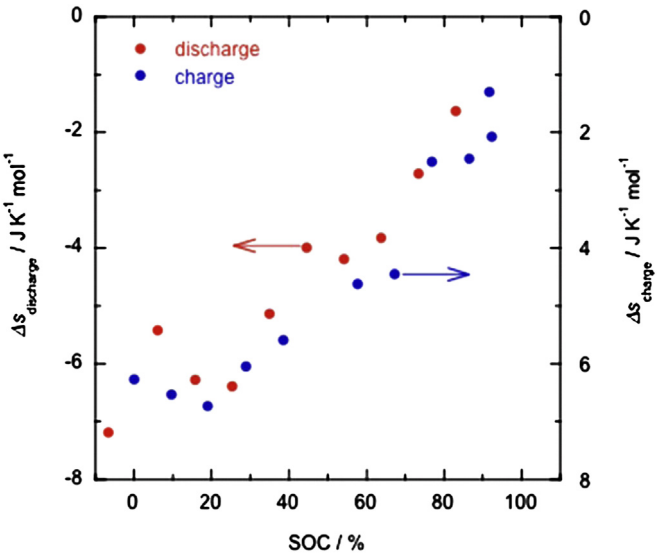

Fig. 6. Partial entropy change Δs (J K^{-1} mol^{-1}) of cell reaction of cell C.

polarizations, $\eta(I)$, at the interfaces between both electrodes and the electrolyte. In order to confirm that the generated heat from the sample cells could be described by Eqs. (1) and (2), V_ocv and its temperature derivative were measured by intermittent charging and discharging combined with a temperature scan during the rest time when the circuit was open. The details of the method are given in Ref. [18]. Fig. 5 shows a plot of the measured V_ocv of the sample cell C as compared with the working voltage during constant current charging and discharging at 45 mA. A small hysteresis can be observed in the low-SOC region between the V_ocv measured by intermittent charging and discharging, which is a typical characteristic of cells using a hard carbon negative electrode. The difference between the working voltage and V_ocv corresponds to the overvoltage, η, and is plotted in Fig. 6. For both charging and

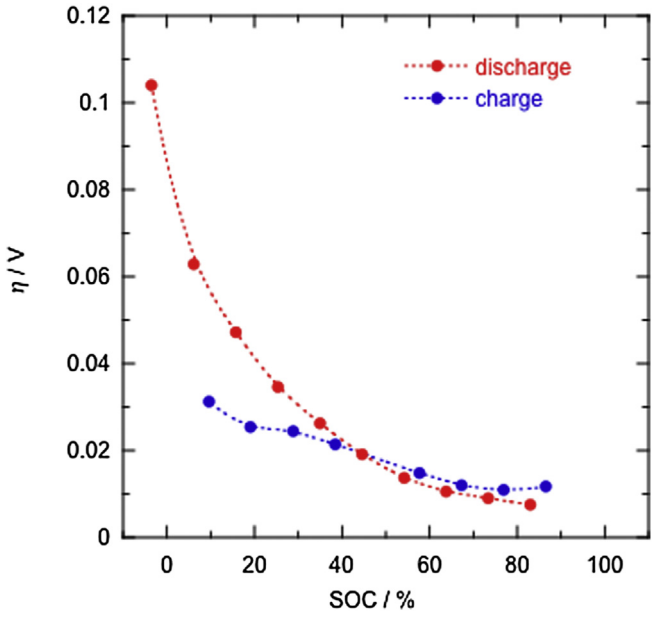

Fig. 5. Overvoltage η (V) of cell C during constant current charging and discharging at 45 mA.

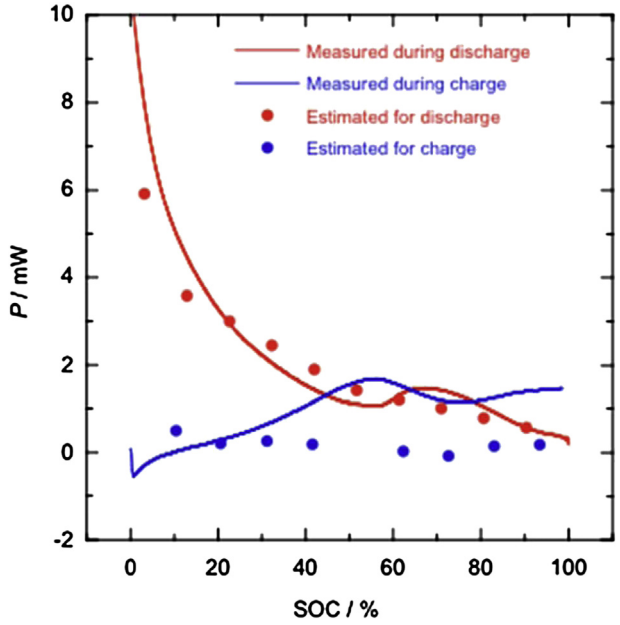

Fig. 7. Heat generation curves P (mW) of cell C during constant current charging and discharging at 45 mA, and the estimated values from the overvoltage η and the partial entropy change Δs of the cell reaction.

discharging, a larger overvoltage is exhibited in the lower-SOC region. A particularly large overvoltage is observed during the final period of discharging. The partial entropy change of the cell reaction, Δs(SOC), evaluated from the temperature derivative of V_{ocv} is plotted in Fig. 6. This value is negative during the discharging reaction and positive during the charging reaction. However, the absolute values are almost the same for both charging and discharging at a given SOC, suggesting that the cell reaction on the whole proceeds reversibly. Using Eq. (2) with the results of Figs. 5 and 6, heat generation values are calculated for 45 mA constant current charging and discharging, and the results are plotted in Fig. 7 against the measured values from calorimetry. For the charging reaction, a large divergence is observed between the calculated and the measured values. This is similar to the results of a past study using a commercial LIB with a hard carbon negative electrode [19]. The large hysteresis of the voltage shown in Fig. 4 causes energy loss in a charging and discharging cycle, and the corresponding energy seems to be dissipated from the cell mainly during the charging process and the final period of discharging. Thus, the heat of the cell using a hard carbon electrode during charging cannot be described simply by Eq. (1) or (2). On the other hand, the measured heat during discharging shows good agreement with the calculated value, as shown in Fig. 6.

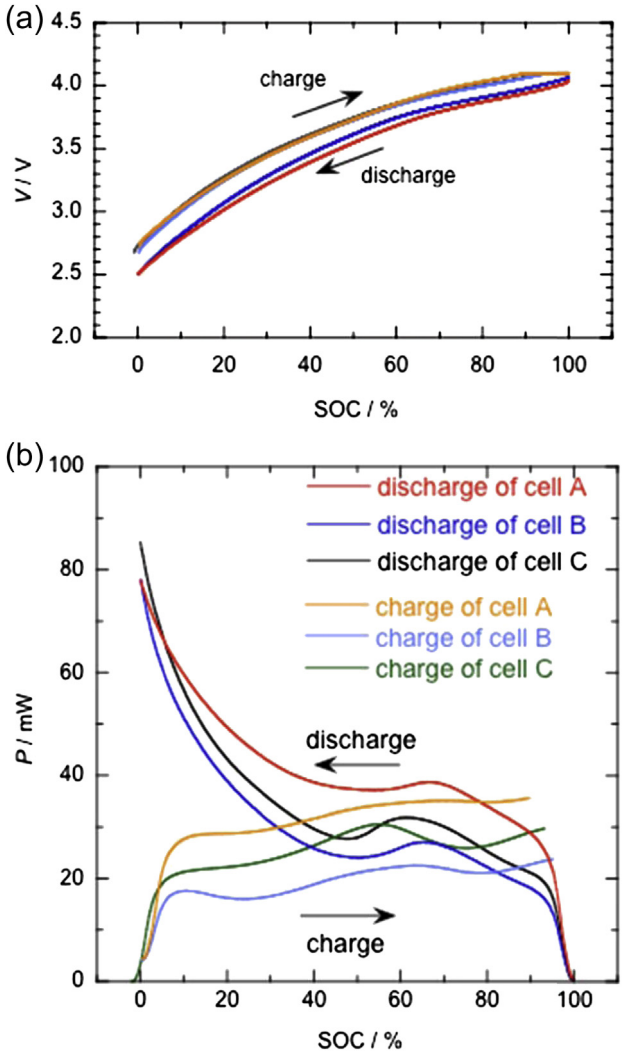

Fig. 8. (a) Voltage V (V) and (b) heat flow P (mW) profiles of the sample cells during constant current charging and discharging at 450 mA. The temperature is 25 °C.

Fig. 8 shows the voltage and heat generation profiles of the sample cells during constant current charging and discharging at 450 mA, which approximately corresponds to a 1 C rate. At such a high C-rate, the hysteresis between the charging and discharging voltages (shown in Fig. 4, which is a low-rate case) is not as large as when the C-rate is low, for all the sample cells. Since the voltage hysteresis is thought to be caused by cell reactions with an extremely slow rate of reversible chemical reaction in the hard carbon electrode [19,20], it might become small in the high-rate condition, where the slow rate chemical reaction could not proceed sufficiently.

The heat generation behavior of the degraded cells at a high rate of charging and discharging is dependent on the samples, as shown in Fig. 8. With both charging and discharging, the largest heat value is observed for the cell stored at 50 °C, and the smallest for the cell stored at 25 °C. This observation agrees with the DC resistance and the power capability values in Table 3 and the $R_{s,\ aft}$ values in Table 4. Although estimation of heat from the sample cells during charging is difficult because of the influence of voltage hysteresis, the heat during discharging is approximately described by Eq. (2), as already mentioned. In this equation, while P_s is linearly related to the current, P_r has a higher-order relation with the current because the overvoltage also changes with the current. Hence, even if P_s is dominant in low-rate charging and discharging, P_r becomes more dominant in the high-rate condition. Thus, it can be concluded that more degraded cells that undergo larger increases in resistance exhibit greater heat dissipation at high rates of charging and discharging. It was suggested earlier that in our sample cells, an increase in the solution resistance due to leakage of the electrolyte during storage is the main cause of power fading. Improving the sealing of the cell would be an effective measure to suppress temperature increase during cycling for long-time usage.

4. Conclusion

Calorimetry was applied to characterize the heat generation behavior during the charging and discharging of lithium-ion batteries degraded by long-time storage. At high rates of charging and discharging, the more degraded LIBs showed larger heat generation related to an increase in the overvoltage. The main reason for the striking increase in solution resistance in the battery stored at 50 °C could be leakage of the electrolyte solution. In the thermal design of LIBs, we have to take into account battery characteristics not only for the fresh state but also for the post-degradation state, particularly when the battery is deployed in high-rate applications.

Acknowledgments

This work was supported by “The Lithium-Ion and Excellent Advanced Batteries Development (Li-EAD) Project” of the New Energy and Industrial Technology Development Organization (NEDO) in Japan.

References

[1] Japanese Industrial Standards Committee, JIS C8714, Safety Tests for Portable Lithium Ion Secondary Cells and Batteries for Use in Portable Electronic Applications (2007).
[2] Underwriters Laboratories Inc., UL1642, Ul Standard for Safety for Lithium Batteries (1995).
[3] Y. Saito, J. Power Sources 146 (2005) 770–774.
[4] H. Kobayashi, M. Shikano, S. Koike, H. Sakaebe, K. Tatsumi, J. Power Sources 174 (2007) 380–386.
[5] M. Shikano, H. Kobayashi, S. Koike, H. Sakaebe, E. Ikenaga, K. Kobayashi, K. Tatsumi, J. Power Sources 174 (2007) 795–799.
[6] M. Rahman, Y. Saito, J. Power Sources 174 (2007) 889–894.
[7] Y. Saito, M. Rahman, J. Power Sources 174 (2007) 676–680.

[8] D. Mori, H. Kobayashi, M. Shikano, H. Nitani, H. Kageyama, S. Koike, H. Sakaebe, K. Tatsumi, J. Power Sources 189 (2009) 380–386.
[9] M. Shikano, H. Kobayashi, S. Koike, H. Sakaebe, Y. Saito, H. Hori, H. Kageyama, K. Tatsumi, J. Power Sources 196 (2011) 6881–6883.
[10] Y. Saito, M. Shikano, H. Kobayashi, J. Power Sources 196 (2011) 6889–6892.
[11] S. Seki, N. Kihira, Y. Mita, T. Kobayashi, K. Takei, T. Ikeya, H. Miyashiro, N. Terada, J. Electrochem. Soc. 158 (2011) A163–A166.
[12] S. Seki, Y. Mita, T. Kobayashi, K. Takei, T. Ikeya, H. Miyashiro, N. Terada, CRIEPI REPORT, Q02023 (2010).
[13] J.R. Dahn, T. Zheng, Y. Liu, J.S. Xue, Science 270 (1995) 590–593.
[14] Y. Saito, K. Takano, K. Kanari, T. Masuda, Bull. Electrotech. Lab. 60 (1996) 771–778.
[15] W.R. McKinnon, J.R. Dahn, J.J. Murray, R.R. Haering, R.S. McMillan, A.H. Rivers-Bowerman, J. Phys. C Solid State Phys. 19 (1986) 5135–5148.
[16] G.M. Bergman, S.J. Ebel, E.S. Takeuchi, P. Keister, J. Power Sources 20 (1987) 179–185.
[17] J.J. Murray, A.K. Sleigh, W.R. McKinnon, Electrochim. Acta 36 (1991) 489–498.
[18] K. Takano, Y. Saito, K. Kanari, K. Nozaki, K. Kato, A. Negishi, T. Kato, J. Appl. Electrochem. 32 (2002) 251–258.
[19] Y. Saito, K. Takano, K. Kanari, K. Nozaki, Mat. Res. Soc. Symp. Proc. 496 (1998) 551–556.
[20] Y. Saito, K. Kanari, K. Takano, K. Nozaki, J. Power Sources 81–82 (1999) 913–917.